Journal of Membrane Science 685 (2023) 121967

Contents lists available at ScienceDirect

Journal of Membrane Science

journal homepage: www.elsevier.com/locate/memsci

The role of solvent temperature and gas pressure on CO_2 mass transfer during biogas upgrading within porous and dense-skin hollow fibre membrane contactors

B. Luqmani [a], A. Brookes [b], A. Moore [c], P. Vale [d], M. Pidou [a], E.J. McAdam [a,*]

[a] Cranfield Water Science Institute, Vincent Building, Cranfield University, Bedfordshire, MK43 0AL, UK
[b] Anglian Water, Block C-Western House, Peterborough Business Park, Peterborough PE2 6FZ, UK
[c] Northumbrian Water, Boldon House, Wheatlands Way, Durham DH1 5FA, UK
[d] Severn Trent Water, 2 St. Johns Street, Coventry CV1 2LZ, UK

ARTICLE INFO

Keywords:
Asymmetric
Carbon capture (CCS)
Water
Biomethane
Selectivity
Permeability

ABSTRACT

Biogas upgrading uniquely requires pressurisation of hollow fibre membrane contactors (HFMC) to be competitive with classical water absorption, and when complemented with an ambient industrial temperature range, these conditions will determine CO_2 mass transport phenomena that are distinct dependent upon whether microporous or nonporous membranes are used. This study therefore examines the independent and concomitant role of temperature and pressure in determining CO_2 mass transport, and selectivity, within microporous and nonporous HFMC. At low solvent temperatures, higher CO_2 flux was achieved which indicates that solvent solubility is more critical than CO_2 diffusivity to enhancing mass transport. Low temperatures also favoured mass transfer within the microporous membrane, explained by the reduction in solvent vapour pressure which limited pore wetting by condensation. In contrast, the nonporous membrane exhibited poorer mass transfer at low temperatures due to a decline in dense polymer permeability. Crucially in this study, neither wetting of the microporous membrane or plasticisation of the nonporous membrane were observed following pressurisation. Consequently, CO_2 flux increased in proportion to the applied pressure for both membrane types, emphasising the critical role of pressurisation in augmenting process intensification for biogas upgrading which is typically facilitated at pressures of 7–10 bar. Resistance-in-series analysis illustrated how pressurisation reduced gas-phase resistance, and subsequently enhanced selectivity. Consequently, an outlet gas quality of 98% methane could be achieved within a single microporous module at 4.5 bar, meeting the industrial standard for biomethane whilst reducing solvent requirements, separation energy and methane losses. Comparable behaviour was observed during pressurisation of the nonporous membrane, but with a less significant benefit to CO_2 mass transfer and selectivity, ostensibly due to the resistance imparted by the dense polymer. When considered collectively, low solvent temperature and high gas pressure enhance process intensification subsequently reducing process size (e.g., membrane area) and separation energy, while also advancing selectivity to deliver a gas product at the composition required for biomethane with minimum methane losses, which are critical factors in demonstrating microporous HFMC as an industrially competitive solution for biogas upgrading.

1. Introduction

Biogas produced from the anaerobic digestion of organic rich waste can be upgraded into biomethane (95–98% methane) to decarbonise existing natural gas infrastructure or as a sustainable 'drop-in' transport fuel by replacing fossil derived gasoline and diesel [1,2]. Biomethane is therefore seen as a critical resource for the decarbonisation of heat and transport in Europe [3,4]. Pressurised water absorption (PWA) uses water to facilitate carbon dioxide (CO_2) absorption from biogas in packed columns and represents one third of biomethane installations across Europe [5,6]. Hollow fibre membrane contactors (HFMC) are an emerging technology that can similarly mediate CO_2 absorption for biogas upgrading. In HFMC, the gas and liquid are separated by a gas permeable membrane to facilitate non-dispersive gas transfer between

* Corresponding author.
E-mail address: e.mcadam@cranfield.ac.uk (E.J. McAdam).

https://doi.org/10.1016/j.memsci.2023.121967
Received 12 July 2023; Received in revised form 26 July 2023; Accepted 27 July 2023
Available online 1 August 2023

phases, thus avoiding channelling, flooding, foaming and entrainment that are common challenges for packed columns [7]. This enables higher gas loading rates to be applied resulting in smaller installed capacity, while the superior specific surface area in HFMC can enable process intensification of up to fifteen times versus packed columns [8].

A dry microporous membrane layer will offer negligible resistance to CO_2 mass transfer [9]. However, many researchers have observed wetting of the pore structure which can substantially increase membrane resistance due to the lower diffusivity of CO_2 in water [10–12]. For example, pore wetting in polypropylene (PP) hollow fibres resulted in an increase in membrane resistance up to 143,000 s m^{-1} (43% of the overall mass transfer resistance) [11]. [13] reported total pore wetting of microporous HFMC during CO_2 absorption into 30% MEA at 35 to 65 °C. During carbon capture, the elevated flue gas temperature (>50 °C) will naturally raise the solvent temperature due to efficient heat transfer across the HFMC [14,15]. Investigation of CO_2 absorption at lower solvent temperatures is relevant for biomethane production (<30 °C), since biogas is produced at ambient conditions [16]. Lowering solvent temperature improves gas solubility which can increase CO_2 flux [17–19]. However, this will also increase methane flux into the solvent (i.e., methane 'slip'). As the increase in solubility is proportionate to temperature, selectivity of the binary gas mixture (CO_2/CH_4) should not be affected but the increase in methane slip will have financial and environmental implications [8]. Reduced pore wetting has also been observed at lower temperatures [18,20]. This has been related to an increase in solvent surface tension, since this increases the pore pressure required for solvent breakthrough. The reduction in vapour pressure may also mitigate pore wetting, by reducing the probability for capillary condensation [14], analogous to the reduction of ammonia slip at lower temperatures during chemical absorption [21]. Since transmembrane pressure is not consistently reported and wetting has been observed well below the theoretical breakthrough pressure, confirmation of the link between temperature and wetting in microporous membranes has yet to be demonstrated [10,18,20].

For hollow fibre membrane contactors to be competitive with packed columns, they must also be capable of pressurisation, as pressure is used to improve absorption capacity, reduce solvent mass flow to regeneration, minimise methane slip and advance the co-absorption of trace gases (e.g. siloxanes, hydrogen sulphide and ammonia) [22,23]. Landfill gas, which can contain raised oxygen concentrations (0.5–1%vol), may require an additional oxygen separation stage since it is sparingly soluble and absorption is negligible even at high pressures (20–25 bar) [24,25]. Following biogas upgrading, the biomethane product must be pressurised for injection into the gas network, which is typically rated at 2–7 bar [26,27]. Consequently, pressurising the gas phase upstream of biogas upgrading prepares the gas phase for injection, while taking economic advantage of pressure to reduce capital and operating cost. Pressurisation of HFMC is therefore needed to achieve competitive process intensification to conventional PWA. However, limited data is available on the influence of pressure on CO_2 absorption within HFMC, particularly for biogas upgrading [10]. demonstrated that increasing gas pressures up to 20 bar led to a proportional enhancement in CO_2 flux across a single microporous hollow fibre, due to the increase in volumetric CO_2 concentration. Pressure was not observed to reduce overall mass transfer resistance, while membrane resistance was observed to be constant, indicating that pore wetting was avoided by sustaining a constant transmembrane pressure [10]. These experiments were conducted in semi-batch mode, with a continuous flow of solvent used to absorb CO_2 from a reservoir which sustained CO_2 partial pressure leading to a negligible gas-phase mass transfer resistance (<0.5%) [10]. During biomethane production, the partial pressure of CO_2 will reduce by 95% and there is evidence that gas-phase resistance can become more significant to mass transfer possibly due to the reduction in partial pressure and decrease in gas velocity across the length of the HFMC, which may have a more significant effect for biogas than flue gas due to the higher initial CO_2 partial pressure [28]. The extent to which pressure governs mass transfer within each phase of a microporous HFMC, and its implications for gas quality in a binary separation have not been explored to date.

To prevent pore wetting and stabilise mass transfer during CO_2 absorption, a thin layer of gas-permeable dense polymer can be incorporated on to the membrane surface to produce a nonporous HFMC [29,30]. When compared to microporous HFMC, gas transport is more dependent on the thickness and permeability of the polymer layer [29]. This transport mechanism is expected to mitigate methane slip into the solvent since the polymer can introduce an inherent selectivity toward CO_2 (e.g. poly(4-methyl-1-pentene), thus enhancing CO_2/CH_4 selectivity [8,31,32]. While nonporous HFMC offer several advantages, gas permeability is likely to decline at lower temperatures [13]. When in contact with an aqueous solvent, lower polymer permeability (e.g. Teflon AF1600, PTMSP and PIM 1) has been observed than for dry conditions, which may infer the competitive sorption of water vapour within the polymer [13,33,34]. Whilst the dense polymer poly (4-methyl-1-pentene) has been explored widely for gas-phase separations due to its high permeability and chemical resistance [35], permeability data in the presence of aqueous solvents is unavailable. Permeability can be expected to be independent of pressure, but a decline in CO_2 permeability and selectivity was observed during the pressurisation of ultrathin (0.1–0.2 μm) polyethersulfone-polyimide nonporous hollow fibres due to the suspected plasticisation of the dense polymer [36]. However, when studying a poly(phenylene oxide) nonporous HFMC for the absorption of CO_2 into water at 2.5 bar, a membrane resistance of 1970 s m^{-1} was reported which is comparable to the mass transfer resistance determined for a microporous HFMC [8,28]. This suggests that pressurisation did not affect polymer permeability, although higher pressures within the range relevant for biogas upgrading were not explored.

The aim of this research is to compare microporous and nonporous HFMC at low temperatures and high pressures which represent critical parameters for biomethane production. Specific objectives are to: (i) characterise the role of solvent temperature (5–35 °C) on membrane resistance and CO_2 transport mechanisms within microporous and nonporous HFMC to aid material selection for biomethane production; (ii) determine how pressure (1.1–4.5 bar) informs on mass transfer behaviour across the three discrete phases within the system, with emphasis on the susceptibility of microporous and nonporous membranes to the implicit risks of pressurisation on gas permeability; and (iii) evaluate how temperature and pressure modify selectivity, including gas product quality and methane slip from a binary CO_2/CH_4 gas comprised of a high CO_2 partial pressure.

2. Materials and methods

2.1. Experimental set-up

The experimental setup was developed to evaluate CO_2 mass transfer within transverse flow membrane contactors comprising microporous polypropylene hollow fibres with a maximum pore size of 0.1 μm, or nonporous hollow fibres with an asymmetric structure comprising a 1 μm dense poly(4-methyl-1-pentene) layer (3 M Industrial Group, Charlotte, USA) (Table 1). The microporous module contained 10,200 fibres and provided a total internal surface area of 1.2 m^2. Each fibre had an internal diameter, wall thickness and length of 240 μm, 30 μm and 0.16 m respectively. The nonporous module contained approximately 8500 fibres and provided a total internal surface area of 0.9 m^2. Each fibre had an internal diameter, wall thickness and length of 240 μm, 89 μm and 0.16 m respectively. Pure carbon dioxide or a 50/50 volumetric blend of carbon dioxide and methane (CO_2, 99.7%; CH_4, 99.995%, BOC gases, Ipswich, UK) was introduced into the HFMC lumen (0.01–5.0 L min^{-1}, Roxspur Measurement and Control Ltd., Sheffield, UK) and deionised water (15 MΩ cm) was pumped counter-currently through the shell-side (AD4/90, Xylem Inc., New York, USA) (Fig. 1). Gases were supplied at

Table 1
Material and structural properties of hollow fibre membrane contactors.

	Microporous HFMC	Nonporous HFMC
Dense-skin (μm)[a]	N/A	~1
Internal fibre diameter (μm)[a]	240	200
Fibre wall thickness (μm)[a]	30	89
Fibre length (m)[a]	0.16	0.16
Tortuosity (−)[a]	0.4	–
Porosity (−)[a]	2.5	–
No. fibres (−)[b]	~10,200	~8500
Total surface area (m^2)[b]	1.2	0.9
Specific surface area ($m^2\ m^{-3}$)[b]	1860	1293
Contact angle (°)[c]	122	–
Geometric pore factor (−)[d]	0.56	–
Max. pore size (μm)[e]	0.1	–
Breakthrough pressure (bar)[f]	8.9 (5 °C) 8.4 (35 °C)	N/A

[a] Data supplied by manufacturer.
[b] Based upon internal fibre diameter.
[c] Lv et al. (2010).
[d] Bavarella. (2018).
[e] Heile et al. (2014), (Bavarella, 2018).
[f] Based upon pure water.

approximately 22 °C, and gas and liquid temperatures monitored using k-type thermocouples (±1.5 °C, RS Components, Corby, UK). Shell-side water temperature was modified using a thermostatic recirculating water bath (LT Ecocool 150, Grant Instruments, Cambridge, UK) to permit solvent temperatures ranging 5 to 35 °C. Gas and liquid pressures were monitored across the system (DPG1001B-100G, ±0.10% full scale, Omega Engineering Ltd., Manchester, UK) and controlled using throttling valves at the lumen and shellside outlets respectively (SS-4MA-MH, Swagelok, Kings Langley, UK) to ensure gas pressure between 1.1 and 4.5 bar could be used. Gas bubbling was observed when pressure equalised across the membrane and so a liquid-side overpressure was established of between 0.2 and 0.4 bar with care taken not to exceed the breakthrough pressure at the liquid inlet (Table 1) [10]. Outlet gas flow was measured at atmospheric pressure using volumetric bubble flowmeters (50 mL, ±2% full scale, Restek, Bellefonte, USA; 1000 mL, Model 311, ±2% full scale, Blandford Forum, UK) and normalised to the gas inlet temperature and pressure (Appendix A.1.). Gas outlet composition was monitored using an in-line infrared CH_4 analyser (BCP–CH_4, <0.5% full scale, BlueSens gas sensor GmbH, Herten, Germany). Following each experiment, the lumen underwent a 45-min drying step with compressed air at 30 L min^{-1} to restore hydrophobicity [37]. In this work, mild drying conditions were applied (20 °C, 1 bar) and reproducible results throughout experimentation indicated that membrane properties

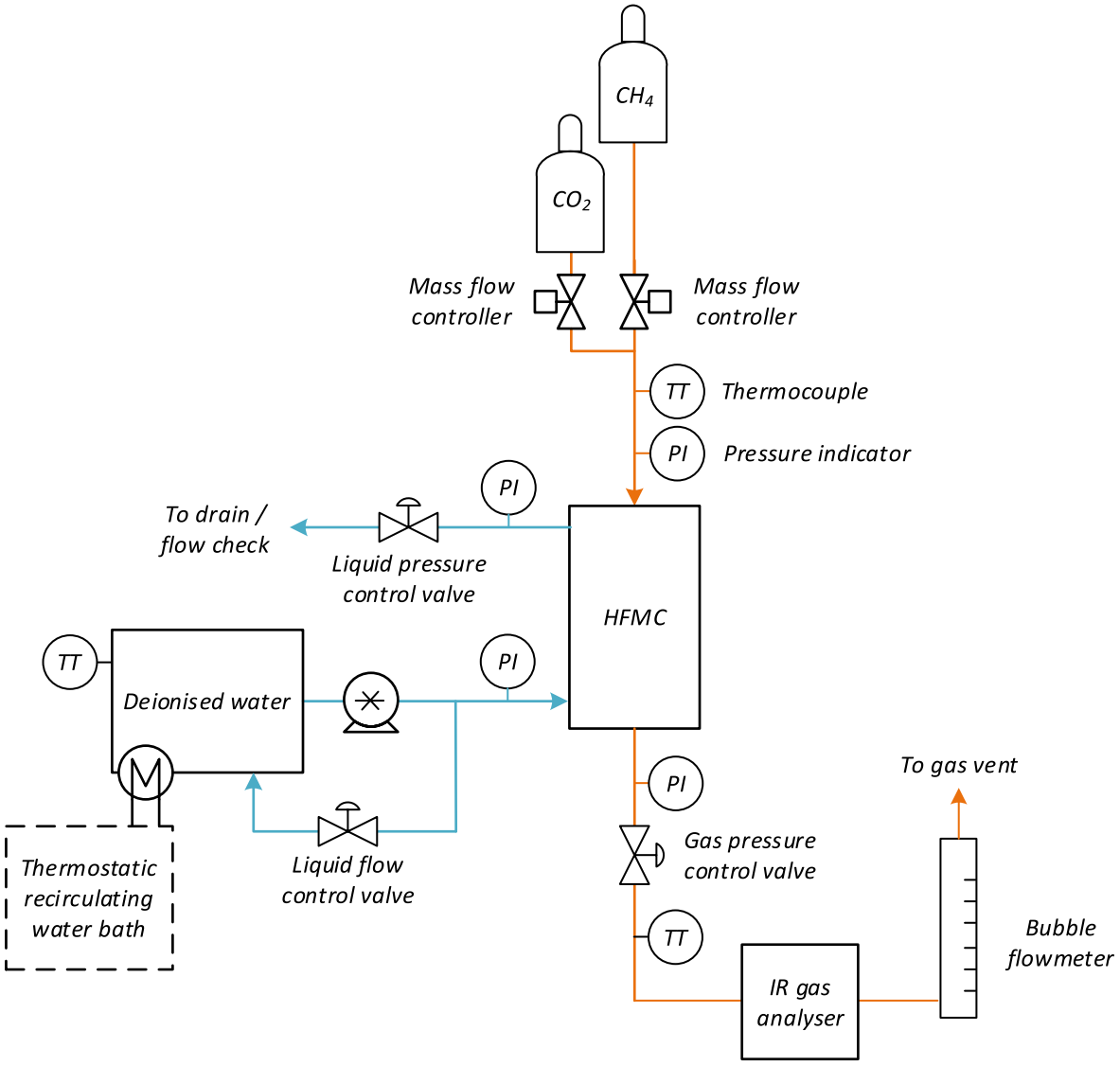

Fig. 1. Experimental setup for gas-liquid absorption in HFMC.

were unaffected by cycles of wetting and drying. Each data point was replicated, and the mean reported with standard deviation represented by the error bars. To discriminate the role of temperature on membrane wetting, solvent exposure during the resistance in series analyses was standardised by allowing the system to stabilise for 2 min at each operating condition prior to data collection.

2.2. Experimental analysis

Experimental CO_2 capture ratio [38] was determined using:

$$\eta_{CO2} = \frac{Q_{g,in}\, y_{CO2,in} - Q_{g,out}\, y_{CO2,out}}{Q_{g,in}\, y_{CO2,in}} \quad (1)$$

where η_{CO2} is the CO_2 capture ratio (−); Q_g is the gas flowrate ($m^3\ s^{-1}$); y_{CO2} is the CO_2 fraction in the gas-phase (%vol); and subscripts 'in' and 'out' refer to conditions at the membrane inlet and outlet respectively. Experimental CO_2 flux and overall mass transfer coefficients [38] were calculated as:

$$J_{CO2} = \frac{Q_l\, C_{l,out}}{a} = K_{ov}\Delta\left(C_l^* - C_l\right)_{lm} = K_{ov}\Delta\left(HC_g - C_l\right)_{lm} \quad (2)$$

$$\Delta\left(HC_g - C_l\right)_{lm} = \frac{\left(HC_{g,in} - C_{l,out}\right) - \left(HC_{g,out} - C_{l,in}\right)}{\ln\left[\frac{HC_{g,in} - C_{l,out}}{HC_{g,out} - C_{l,in}}\right]} \quad (3)$$

where J_{CO2} is the flux (mol $m^{-2}\ s^{-1}$); Q_L is the liquid flowrate in and out of the shellside ($m^3\ s^{-1}$); a is the total surface area based upon fibre internal diameter (m^2); K_{ov} is the overall mass transfer coefficient for CO_2 (m s^{-1}); H is the dimensionless Henry's law partition coefficient for CO_2 in water for a given temperature (−) (Table 2); C_g is the gas-phase CO_2 concentration for a given pressure and temperature (mol m^{-3}) (Appendix A.2.); and C_l is the liquid-phase CO_2 concentration (mol m^{-3}).

A resistance-in-series approach was applied to separate the overall mass transfer resistance, $1/K_{ov}$ (s m^{-1}) into the three constituent resistances (gas, liquid and membrane) (Equation (4)). Whilst this methodology was originally developed for flat sheet membranes, it has been widely applied for description of mass transfer within membrane contactors with cylindrical fibre geometry [9,38–40].

$$\frac{1}{K_{ov}} = \frac{1}{k_g} + \frac{1}{k_m} + \frac{1}{k_l} \quad (4)$$

where $1/k_g$, $1/k_L$, and $1/k_m$ represent mass transfer resistance for the gas-phase, membrane and liquid-phase respectively (s m^{-1}).

Liquid-phase mass transfer resistances were estimated using a shell-side Graetz-Leveque solution for transverse-flow HFMC (Equation (5)) first developed for liquid-liquid extraction [41]. The Reynolds number, *Re* (−), and shell-side hydraulic diameter, d_h (m), were calculated assuming parallel flow within the shell-side in accordance with previous literature [40,42]. Since both microporous and nonporous modules had the same internal geometry, *Re* was equivalent across the liquid velocity range. The Graetz-Leveque solution was determined to accurately predict liquid-phase mass transfer resistance, under conditions where the liquid Graetz number was greater than 15 (Appendix B).

$$Sh = 0.56\, Re^{0.62}\, Sc^{0.33} = \frac{k_l d_h}{D_{CO2,l}} \quad (5)$$

where Sh is the Sherwood number (−); Sc is the Schmidt number (−) and $D_{CO2,l}$ is the diffusivity of CO_2 in the solvent at a given temperature (Table 2) ($m^2\ s^{-1}$).

Membrane mass transfer resistance was estimated from the experimental data using the Wilson plot method [38]. Membrane resistance for the microporous HFMC, $1/k_{m,p}$ (s m^{-1}), enabled estimation of wetted pore fraction, x (−), for each condition (Equation (6)) [43]. This approach is based upon the principle that the diffusivity of CO_2 in gas-filled pores is 3-4 orders of magnitude greater than in water-filled pores at 5–35 °C and so the membrane resistance will decline as water progresses along the pore length. Notably, this assumes all pores are uniformly wetted across the contactor, which is unlikely in practice due to pore size distribution, but this does provide useful approximation for comparing the magnitude of wetting across different conditions [43].

$$\frac{1}{k_{m,p}} = (1-x)\frac{\tau_m \delta_w}{D_{CO2,g} \in_m} + x\frac{\tau_m \delta_w}{H\, D_{CO2,l} \in_m} \quad (6)$$

where τ_m is membrane tortuosity (−); δ_w is the porous wall thickness (m); $D_{CO2,g}$ is the diffusivity of CO_2 in the gas-phase ($m^2\ s^{-1}$); ε_m is the membrane porosity (−).

Membrane resistance for the nonporous HFMC, $1/k_{m,d}$ (s m^{-1}), permits estimation of the permeability for the dense polymer (Equations (7) and (8)). This was in direct contact with the liquid-phase and so it was assumed to approach the solvent temperature via rapid conductive heat transfer [15].

$$\frac{1}{k_{m,d}} = \frac{\tau_m \delta_w}{D_{CO2,g} \in_m} + \frac{v_m \delta_f}{P_{d(SI)}\, R\, T_m} \quad (7)$$

$$P_d = \frac{1}{3.35 * 10^{-11}}\left(\frac{P_{d(SI)}}{v_m}\right) \quad (8)$$

where v_m is the gas molar volume ($m^3\ mol^{-1}$); δ_f is the thickness of the dense polymer layer (m); $P_{d(SI)}$ and P_d represent the CO_2 permeability of the polymer in SI units ($10^5\ m^3\ m\ bar^{-1}\ s^{-1}\ m^{-2}$) and Barrer respectively; R is the molar gas constant ($8.314*10^{-5}\ m^3\ bar\ K^{-1}\ mol^{-1}$) and T_m is the membrane temperature (K).

Table 2
Pure water properties from 5 to 35 °C.

	5 °C	10 °C	20 °C	35 °C
Density (kg m^{-3})[a]	999.9	999.6	998.1	994.0
Dynamic viscosity (10^{-3} N s m^{-2})[a]	1.5	1.3	1.0	0.7
Vapour pressure (kPa)[a]	0.9	1.2	2.3	5.6
CO_2 diffusivity ($10^{-9}\ m^2\ s^{-1}$)[b]	1.1	1.3	1.7	2.5
Schmidt number (−)[c]	1375	1032	600	293
Henry's constant for CO_2, C_L^*/C_G (−)[c,d]	1.5	1.3	1.0	0.7
Henry's constant for CH_4, C_L^*/C_G (−)[c,d]	4.8×10^{-2}	4.4×10^{-2}	3.7×10^{-2}	3.0×10^{-2}

[a] Perry, R. H. and D. W. Green (2007) (some values interpolated).
[b] Engineering Toolbox (2008).
[c] Calculated values.
[d] Sander (2015).

3. Results and discussion

3.1. Microporous and nonporous HFMC influenced strongly by temperature

To simplify mass transfer analysis, initial experiments were undertaken using a pure CO_2 feed gas (99.7%) as this will set gas phase resistance to near zero, leaving only the membrane and liquid phase resistances to be determined [38]. Increasing liquid velocity improved CO_2 flux (Fig. 2), due to a higher rate of solvent renewal at the membrane interface [44]. For each condition, a plateau was approached which represents a reduction in boundary layer thickness and implies that liquid phase resistance was tending toward a minimum (Appendix B) [38]. In both microporous and nonporous membranes, CO_2 flux decreased following an increase in water temperature which modified the solubility constant to restrict the solvent CO_2 capacity (Table 2). Flux across the microporous membrane exhibited a greater sensitivity to temperature, indicating a lower overall resistance to mass transfer (Equation (2)).

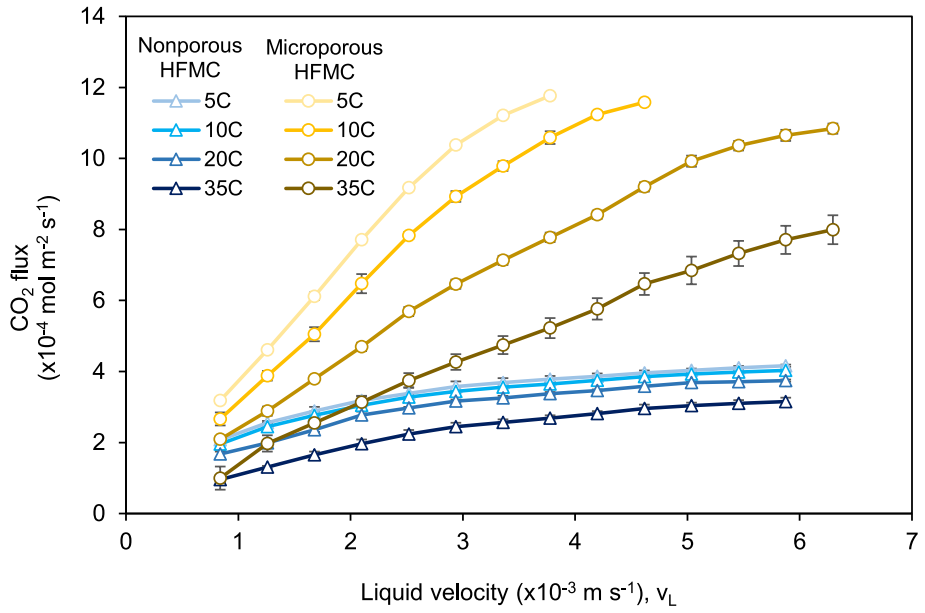

Fig. 2. Impact of solvent temperature on CO_2 flux across microporous (PP) and nonporous (PMP) membranes. Conditions: Pure CO_2 gas feed; v_G = 0.07–0.08 m s^{-1}; P_g = 1.1 bar; gas temperature in = 21 °C.

Mass transfer resistance of the microporous membrane was 385 s m^{-1} at 5 °C, around two orders of magnitude lower than the nonporous membrane (80,700 s m^{-1}) (Fig. 3). As solvent temperature was increased, mass transfer resistance in the microporous membrane increased and was correlated to wetting (Equation (6)). At 5 °C, <0.2% of the pore structure was presumed to be wetted which increased to 7.8% at 10 °C, and 15.4% at 35 °C. Observations of pore wetting at increased temperatures have been attributed to the reduction in solvent surface tension, since this will reduce the pore breakthrough pressure [18,20]. However, the variation in solvent surface tension is minor across the temperature range studied. Consequently, transmembrane pressure (0.2–0.4 bar) represented less than 5% of the pore breakthrough pressure at the highest temperature tested (8.4 bar, based on maximum pore size ~0.1 μm), and so liquid entry was not expected to be the primary mechanism for pore wetting (Table 1). Instead, the exponential increase in water vapour pressure that occurs with an increase in temperature is more likely to have led to partial wetting by the condensation of water vapour in the pore structure (Fig. 4). Capillary condensation will occur when the saturated vapour pressure (P_{sat}) exceeds the equilibrium vapour pressure (P_{eq}) for condensed water within the pores [14]. While the probability of wetting is lower within hydrophobic membranes (Appendix A.3), pore wetting by condensation has been previously reported [11,45,46]. [14] proposed this occurred through minor transients in flowrate and temperature which create local conditions conducive to condensation since P_{eq} responds more quickly than P_{sat} as sufficient time is required for water vapour to diffuse out of

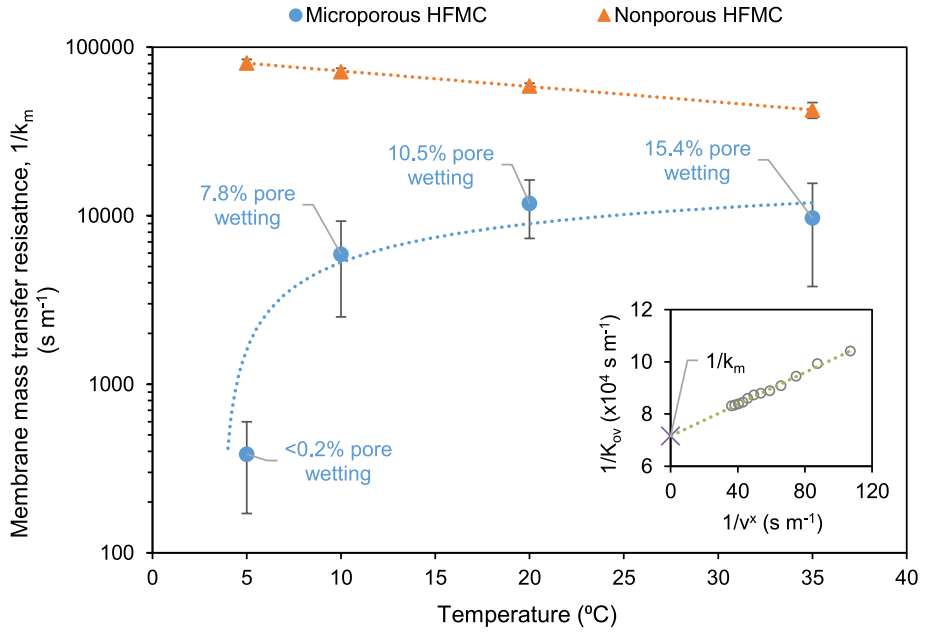

Fig. 3. Impact of solvent temperature on membrane mass transfer resistance for CO_2 within microporous (PP) and nonporous (PMP) membranes. Membrane mass transfer resistances determined using Wilson plot method (example inset for nonporous membrane at 10 °C) Conditions: Pure CO_2 gas feed; v_G = 0.07–0.08 m s^{-1}; P_g = 1.1 bar; gas temperature in = 21 °C. Estimated pore wetting annotated (Equation (6)). Dotted lines added to guide the eye.

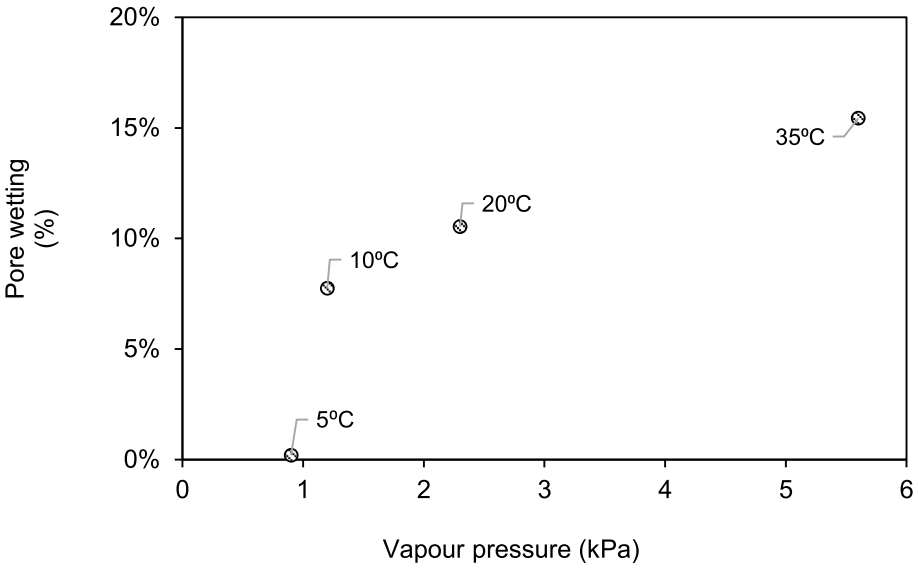

Fig. 4. Influence of water temperature on determined pore wetting and the vapour pressure for pure water. Conditions: pure CO_2 gas feed, v_G = 0.07–0.08 m s^{-1}, P_g = 1.1 bar, gas temperature in = 21 °C. Solvent temperature annotated.

the pores. Notably, a dry gas feed was used in this work in contrast to real biogas which is typically saturated with water vapour [16]. Introduction of a saturated gas phase would limit the vapour pressure gradient across the HFMC and is expected to reduce the probability and extent of wetting by condensation, leading to more favourable mass transfer characteristics in practice.

Mass transfer resistance in the nonporous membrane progressively declined from 80,700 at 5 °C to 42,400 s m^{-1} when water temperature was increased to 35 °C (Fig. 3). The decline in membrane resistance was associated with an increase in CO_2 permeability of the dense polymer (Fig. 5) [13]. In this study, permeability of the polymer was estimated to be 28.8 barrer at 35 °C, which is substantially lower than has been reported for poly(4-methyl-1-pentene) in dry conditions (Table 3) [47–49]. This supports previous observations for dense polymers where permeability is reduced when exposed to water vapour [13,34].

Table 3
Comparison of dense-skin properties.

Polymer	Solvent	Dense-skin	CO_2 permeability[a]	Reference
		μm	barrer	
PMP	DI water	~1.0[b]	29	This study
PMP	None	0.1	61	[47]
PMP	None	0.1–0.2	99	[48]
PMP	None	0.1	93–128	[49]
Teflon AF1600	30% MEA	12	290	[13]
Teflon AF1600	None	12	512	
PTMSP	30% MEA	2	31,100	
PTMSP	None	2	632	

[a] Reported at 35 °C.
[b] Provided by manufacturer.

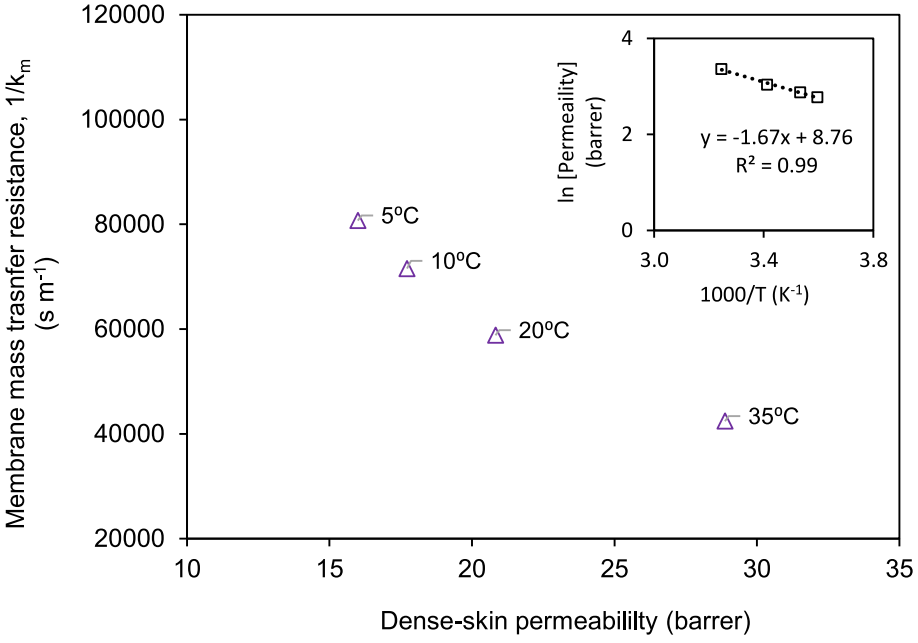

Fig. 5. Influence of dense-skin permeability on membrane resistance for PMP (inset: graphical method for determining dense-skin activation energy, E_a). Conditions: pure CO_2 gas feed, v_G = 0.07–0.08 m s^{-1}, P_g = 1.1 bar, gas temperature in = 21 °C. Solvent temperature annotated.

Temperature and permeability can be related using an Arrhenius expression, in which the activation energy is a compound parameter used to characterise the overall temperature dependence for the polymer [50] (Appendix A.4.). An activation energy of 13.9 kJ mol^{-1} was determined from the experimental data which compares closely to literature for poly(4-methyl-1-pentene) (15.2 kJ mol^{-1}) [48]. This indicates that the impact of competitive sorption on permeability was consisent across the temperature range, despite variation in water vapour pressure; which also then implies that wetting in the porous portion of the asymmetric wall by capillary condensation can be assumed to be negligible within the conditions studied. Therefore, in contrast to the microporous membrane, operating at low temperatures where water vapour transport is limited does not offer any advantage to mass transfer within the nonporous membrane. Distinct gas transport properties have therefore been demonstrated for microporous and nonporous membranes. At low temperatures, the microporous membrane resistance is comparable to a dry membrane and offers negligible mass transfer resistance. For higher temperatures more relevant for carbon capture, the dense polymer permeability increases while wetting begins to dominate within the micropores. Consequently, microporous membranes may favour ambient temperature applications such as biogas upgrading, whereas nonporous membranes may represent the best available technology for carbon capture. Microporous membranes have also demonstrated resilience during exposure to real biogas containing trace volatile organic compounds such as siloxanes, which are simultaneously absorbed into the liquid-phase [16,51]. Permeability data for poly(4-methyl-1-pentene) suggests that the separation layer must be reduced from 1.0 to 0.1 μm for the nonporous membrane to achieve comparable mass transfer (Appendix C). Notably, incorporation of a sub-micron polymer layer requires the addition of a gutter layer which can modify permeability and selectivity and increases complexity for commercial fabrication [52]. Gas pressurisation represents an alternative strategy to enhance mass transfer, that may compensate for high membrane resistances.

3.2. Plasticisation and pore wetting do not limit CO_2 separation under pressure

To determine the effect of pressure on CO_2 mass transfer in HFMC, the gas inlet was initially fixed to pure CO_2 (>99.7%) to provide a consistent gas phase resistance. Consistent overall mass transfer resistance was observed for the microporous and nonporous membranes for pressures up to 4.5 bar (Fig. 6). This is in agreement with the work of [10]. This infers that pore wetting of the microporous membrane was successfully avoided by employing a constant transmembrane pressure of 0.2–0.4 bar across the liquid inlet - gas outlet [10]. Consistent overall mass transfer resistance for the nonporous membrane up to 4.5 bar indicated that the dense polymer did not undergo plasticisation as has been observed for other polymers previously (Fig. 6) [36]. Notably, the relatively thick polymer layer (1 μm) may have provided the mechanical strength to withstand deformation during pressurisation. The density of CO_2 (and its concentration, C_g) will increase in direct proportion with gas pressure (Appendix A.2.). Consequently, an enhancement in CO_2 flux was observed in proportion to the extent of pressurisation (Fig. 7; Appendix A.5.). Pressurised gas-liquid absorption can therefore enable increased gas loading (mol m^{-2} s^{-1}) at the same solvent flow rate which reduces normalised pumping costs, regeneration load and cooling demand.

Gas pressurisation was subsequently investigated using a 50:50 CO_2–CH_4 gas feed to introduce the gas-phase resistance component to CO_2 transport (Fig. 8). Resistance-in-series analysis was based upon consistent membrane resistance observed for the microporous and nonporous membrane following pressurisation. Membrane resistance of the dense polymer is inversely proportional to the pressure dependent permeability parameter (Equation (7)) [15]. Consequently, membrane resistance is a constant that is independent of pressure and from which it can be inferred that the sorption of water vapour did not obviously increase with applied pressure. Liquid phase resistance was also consistent across the pressure range studied for both membranes since the solubility of CO_2 increased in proportion to the pressure applied [17]. However, gas phase resistance reduced following an increase in pressure. This can be explained by the increase in volumetric concentration of CO_2 with pressure which increases the driving force for mass transfer while sustaining the same residence time for separation. For example, in the microporous membrane, $1/k_g$ decreased from 37,800 s m^{-1} at 1.1 bar to 2650 s m^{-1} at 4.5 bar. Consequently, the increased rate of mass transfer complemented by the higher CO_2 solubility in solution, led to a higher methane gas composition at the outlet, which increased from 91 to 98% CH_4 following pressurisation. Comparable behaviour was demonstrated with the nonporous membrane. However, methane concentration at the gas outlet did not increase significantly following pressurisation to 2 bar. This pressure is coincident with the region where $1/k_m$ becomes the dominant resistance to mass transfer (57%). Under these conditions, CO_2 flux is therefore more closely controlled by permeability of the dense polymer layer, and since permeability is proportionate to pressure ($\approx 1/k_m$), a comparable methane outlet concentration was determined above 2 bar. This analysis suggests that the selectivity provided by the dense polymer layer is not beneficial under pressure as has been previously proposed. Instead, it may negate the selectivity advantage that can be imparted when the liquid phase controls mass transfer, as is the case

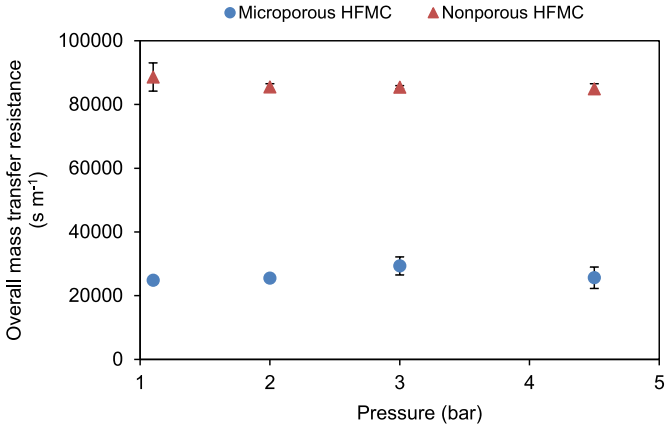

Fig. 6. Impact of gas pressure on overall mass transfer resistance for CO2 transfer across microporous (PP) and nonporous (PMP) membranes. Conditions: Pure CO2 gas feed, vL = 3.2 × 10-3 m s-1, vG = 0.07–0.08 m s-1, solvent temperature = 5–10 °C, gas temperature in = 21 °C.

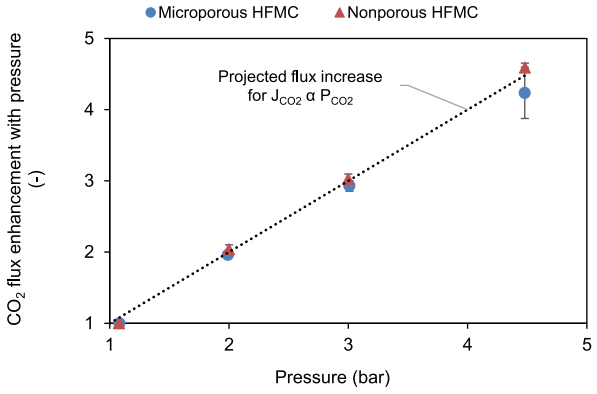

Fig. 7. Impact of gas pressure on flux enhancement factor for CO2 transfer across microporous (PP) and nonporous (PMP) membranes. Conditions: Pure CO2 gas feed, vL = 3.2 × 10-3 m s-1, vG = 0.07–0.08 m s-1, solvent temperature = 5–10 °C, gas temperature in = 21 °C. Dotted line added for proportional flux enhancement with pressure increase relative to 1.1 bar.

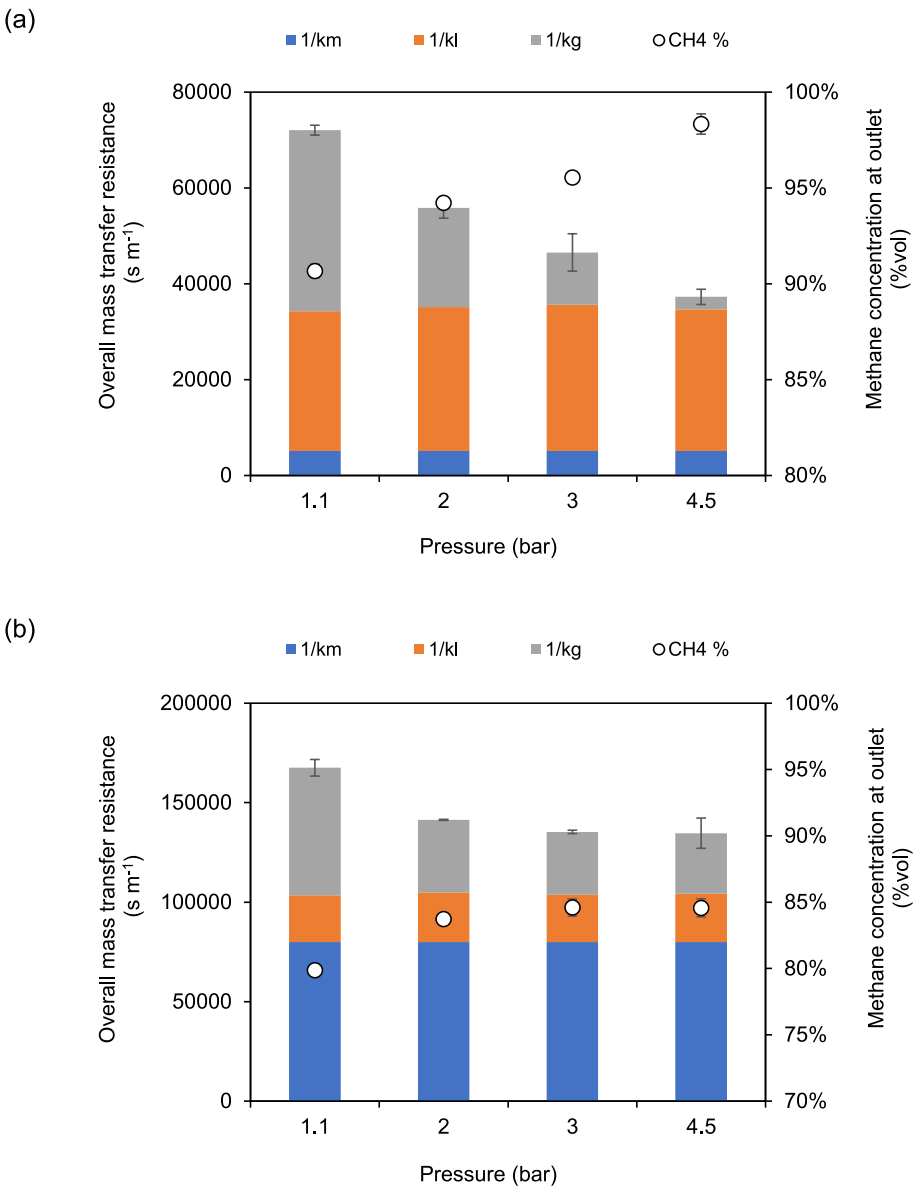

Fig. 8. Impact of gas pressure on mass transfer resistance within: (a) the microporous membrane and (b) the nonporous membrane. Membrane resistances previously determined (Fig. 3) and liquid-phase resistance estimated using Graetz-Leveque solution (Equation (5)). Conditions: 50:50 CO_2/CH_4 gas feed, $v_G = 0.02$ m s^{-1}, $v_L = 1.7 \times 10^{-3}$ m s^{-1}, Gz = 15, solvent temperature = 5–10 °C, gas temperature in = 21 °C.

for the non-wetted microporous membrane.

3.3. *Pressurisation enhances CO_2 selectivity during biogas upgrading*

To characterise how high gas pressures and low solvent temperatures can enhance selectivity, transitions in liquid and gas phase velocity were undertaken to vary mass transfer resistance while modifying gas and solvent loading (Fig. 9). The CO_2 partial pressure declined across the length of the HFMC as indicated by an increase in outlet methane concentration. At a gas velocity of 0.01 m s^{-1} and 1.1 bar pressure, an increase in liquid velocity within the microporous HFMC enabled a peak outlet gas quality of 94%vol at v_L 0.6 $\times$ 10^{-3} m s^{-1}. The enhancement in gas product quality is due to the reduction in liquid phase resistance at higher liquid velocity, which increased CO_2 mass transfer into the solvent [42]. When increasing pressure to 4.5 bar, a higher outlet gas quality could be achieved at a lower liquid velocity than at 1.1 bar. A final product quality of >98% methane was achieved. This conforms with industrial standards for biomethane [1], and demonstrates that pressure is not only advantageous for the rate of mass transfer but can also enhance product quality within the same process scale. Operating at increased pressures will also increase the duty for biogas compressors, therefore representing a compromise between capacity and energy consumption. For example, an increase in biogas pressure from 1 to 10 bar will increase the specific energy consumption for compression by an order of magnitude to approximately 0.1 kWh Nm^{-3} [1]. While increasing gas velocity to 0.02 m s^{-1} raised gas loading and shortened residence time, comparable gas phase quality could be achieved at the highest pressure studied (4.5 bar). However, at lower pressures, the same product quality could not be achieved. The observed enhancement in gas quality with pressurisation is reflected by an increase in selectivity for CO_2 (Fig. 10). Whilst both CO_2 and methane fluxes are enhanced by pressure, there is a greater relative increase for CO_2 due to the associated reduction in gas phase resistance (Fig. 8). As methane is the majority component in the gas phase, gas-phase resistance will be less significant and thus its mass transfer will be less affected by pressurisation [28]. In the nonporous module, higher liquid velocities and lower gas loading

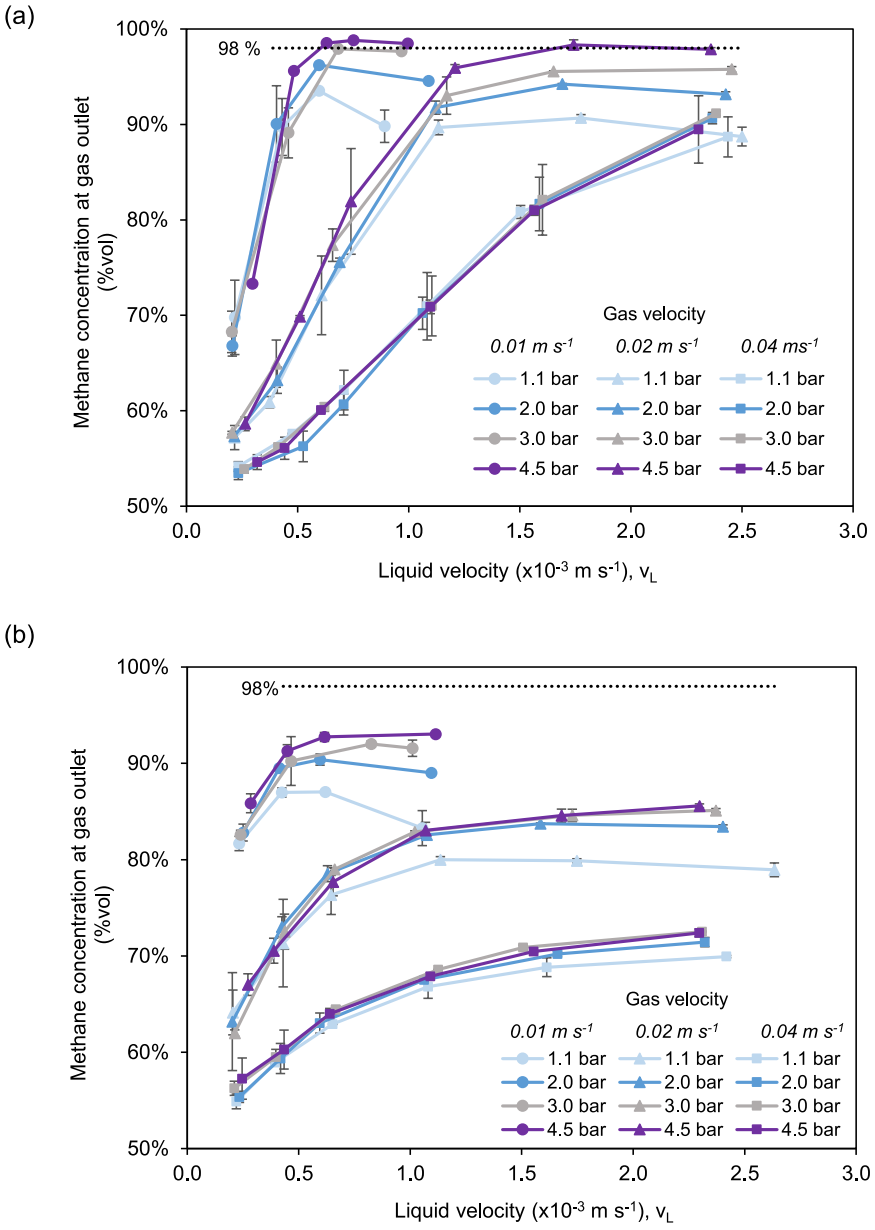

Fig. 9. Impact of gas pressure on methane outlet concentration during binary gas separation within: (a) the microporous membrane and (b) the nonporous membrane. Conditions: gas feed = 0.5/0.5 CO_2/CH_4, solvent temperature = 5–10 °C, gas temperature in = 21 °C. Dotted line represents 98% methane concentration in outlet gas. Absolute pressure values provided.

also increased methane purity of the product gas due to an increased surface renewal within the solvent, and a longer residence time in the gas phase (Fig. 9). Pressure was also demonstrated to increase gas product quality but could not achieve the target concentration specified for biomethane. Pressurisation is therefore not sufficient to offset the reduction in permeability introduced by low temperature. Since $1/k_m$ will primarily control mass transfer at high v_L, where the plateau is approached, the resistance is too high to take advantage of the enhanced selectivity provided by the polymer that must be compensated for either by a reduction in gas flow rate or a reduction in membrane resistance by incorporation of a thinner separation layer, and/or the application of a polymer which exhibits a higher gas permeability.

While methane flux into the solvent is less significant than for CO_2, the 'slip' of methane into the solvent is critically important to biogas upgrading, due to methane constituting a global warming potential 21-times greater than CO_2 [53]. As such, the carbon benefit of biomethane is fully negated when methane losses exceed 13%vol. By increasing pressure, gas quality can be improved at a fixed liquid velocity through the higher CO_2 gas phase partial pressure which enhances CO_2/CH_4 selectivity (Fig. 11). This lowers the energy demand for biogas upgrading, since the liquid velocity will determine the energy consumption required for the compression, chilling and regeneration of the solvent. Methane mass transfer is liquid-phase controlled and so 'slip', as a volume fraction of methane in the raw biogas feed, was relatively consistent across pressures [54]. However, operating at higher pressures will allow recovery of a greater fraction of the slipped methane once the solvent is depressurised ahead of solvent regeneration (so called 'flash') which will lower overall methane losses [22,55]. As such, whilst 11%vol methane slip occurred during biomethane production in the microporous membrane at 4.5 bar, this can be reduced to 4%vol methane losses from the system through downstream recovery. In practice, losses below 1–2%vol are necessary to compete with commercial PWA biogas upgrading plants [56], whilst losses below 0.5%vol are necessary to qualify for financial incentivisation under the German tariff system (EEG

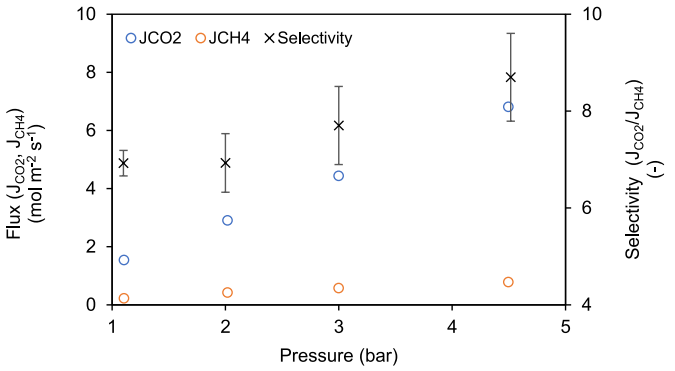

Fig. 10. Influence of pressure on the selectivity of CO_2 transport within the microporous membrane. Conditions: 50:50 CO_2/CH_4 gas feed; $v_G = 0.02$ m s^{-1}, L/G = 1.4; $v_L = 1.7 \times 10\text{-}3$ m s^{-1}; solvent temperature = 5–10 °C, gas temperature in = 21 °C. Absolute pressure values provided.

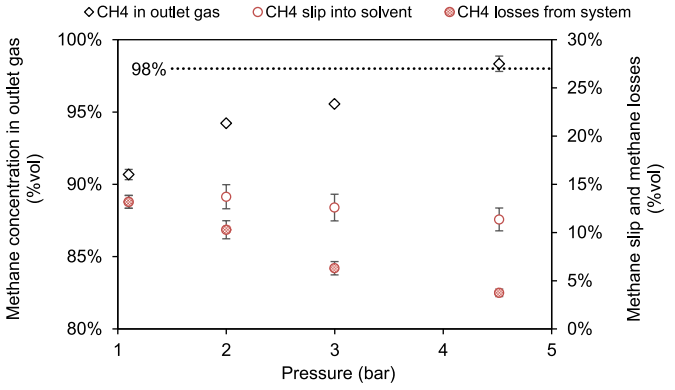

Fig. 11. Impact of gas pressure on outlet gas quality, methane slip and methane losses from the system in the microporous module. Conditions: 50:50 CO_2/CH_4 gas feed, $v_G = 0.02$ m s^{-1}; $v_L = 1.7 \times 10^{-3}$ m s^{-1}; solvent temperature = 5–10 °C; gas temperature in = 21 °C. Ideal dissolved methane recovery estimated for solvent depressurisation to 1.5 bar in a flash vessel. Absolute pressure values provided.

2009) [57]. A further increase in pressure into the range utilised by commercial PWA plants (7–10 bar) may be necessary to lower methane losses to satisfy this incentivisation threshold [5]. This pressure range was evidenced to be feasible for microporous HFMC by Ref. [10] for pure CO_2, and it can be inferred from this study that methane losses will progressively reduce with increasing pressure. However, demonstration of this reduction in slip at higher pressures must be validated for CO_2/CH_4 binary gas separation. This may be complemented by increasing gas loading into the HFMC (Fig. 9), where the increased rate of mass transfer can further enhance CO_2/CH_4 selectivity to sustain product quality (>98%vol) while minimising slip (Table 4).

Volumetric analysis demonstrates the increased gas loading that can be achieved under pressure using considerably less absorption solvent (Fig. 11) and delivering a higher gas quality. However, the volumetric methane 'slip' (rather than losses) is within a comparable range across the pressures tested. This can be explained by the normalisation of L/G for pressure ($m^3_{liquid}\ m^{-3}_{gas}$) which creates a volumetric equivalency for the gas phase, but with a higher molar concentration as pressure is increased (Fig. 12). Consequently, methane slip into the liquid phase is in proportion to the gas phase partial pressure, where the dashed line evidences that an equilibrium is achieved between gas and solvent such that 'slip' can be estimated based on Henry's law for microporous HFMC (Fig. 12b; Appendix A.6.). The equilibrium line also confirms that methane mass transport was not hindered by the microporous membrane [54]. In the nonporous module, methane 'slip' similarly followed equilibrium in proportion with the pressure normalised L/G ratio up to a value of 2–3, after which methane slip was seemingly mitigated (Fig. 12c). This point of transition is consistent with the permeance of methane across the polymer layer approaching 1.5 GPU, close to the limit for poly(4-methyl-1-pentene) (2 GPU) [31,32]. We therefore propose that within this operating region, methane transport is limited by the permeance of the polymer whose properties then determine CO_2/CH_4 selectivity. However, due to the material resistance, higher L/G ratios were required to achieve peak outlet gas quality in the nonporous membrane (~3.6 versus ~1.5 for microporous), increasing slip sufficiently to offset the advantage of the CO_2/CH_4 selectivity provided by the polymer layer. On this basis, microporous membranes maybe preferential for producing biomethane to industrial standards, where low temperatures provide resilience to wetting and high pressures can benefit CO_2/CH_4 selectivity to improve product quality, while minimising methane losses.

Table 4
Performance comparison for binary separation at 4.5 bar, for conditions facilitating 98–99%volCH_4 product quality in microporous HFMC at different gas loading rates.

v_G	v_L	$1/K_{ov}$	Selectivity	CH_4 slip
m s^{-1}	x10^{-3} m s^{-1}	s m^{-1}	J_{CO2}/J_{CH4}	%vol
0.01	0.6	37,300	7.4	13%
0.02	1.7	50,500	8.7	11%

4. Conclusions

This is the first study to investigate the concomitant role of pressure and temperature on CO_2 mass transfer and selectivity within microporous and nonporous membranes, which is critical to advancing HFMC as a next-generation biogas upgrading technology. Based on a systematic examination of temperature, the reduction in wetting observed at lower temperatures is not due to an increase in surface tension, but the reduction in vapour pressure of the solvent which mitigates capillary condensation within the pore structure. The presence of water vapour in real biogas will reduce the vapour pressure gradient across the membrane and is likely to further mitigate the probability and extent of wetting by condensation. Consequently, microporous membranes may be more robust for biogas upgrading than for flue gas carbon capture due to the lower temperature of the gas-phase. Inline chillers are commonly present in biogas pipelines to modify relative humidity of biogas before gas treatment, and so an engineered approach to temperature control may be practically achievable to further enhance separation robustness.

This is the first study to examine pressurisation of a non-stationary binary gas phase within a microporous HFMC and illustrates that despite the significant pressure and velocity transient across the gas-side of the membrane when under pressure, wetting was not instigated when transmembrane pressure was regulated to below the breakthrough pressure. Henry's solubility constant increased in proportion to pressure and as such liquid phase resistance was independent of pressure. Conversely, resistance within the gas film is reduced by increasing pressure due to the increased volumetric concentration which enhances the driving force for mass transfer in proportion to the pressure applied. This mechanism is comparable between microporous and nonporous HFMC, despite mass transfer being primarily controlled by membrane resistance within the poly(4-methyl-1-pentene) separation layer which was constant due to its inverse relationship to the pressure dependent polymer permeability. Although CO_2 permeability within poly(4-methyl-1-pentene) was ostensibly below that reported for dry conditions, membrane resistance was consistent as pressure was increased, suggesting that water vapour sorption and plasticisation behaviour do not significantly inhibit CO_2 permeation. In practice, the raw biogas composition typically approaches saturation. Further study may be required within this more complex matrix to evidence any implications to water vapour flux and sorption behaviour.

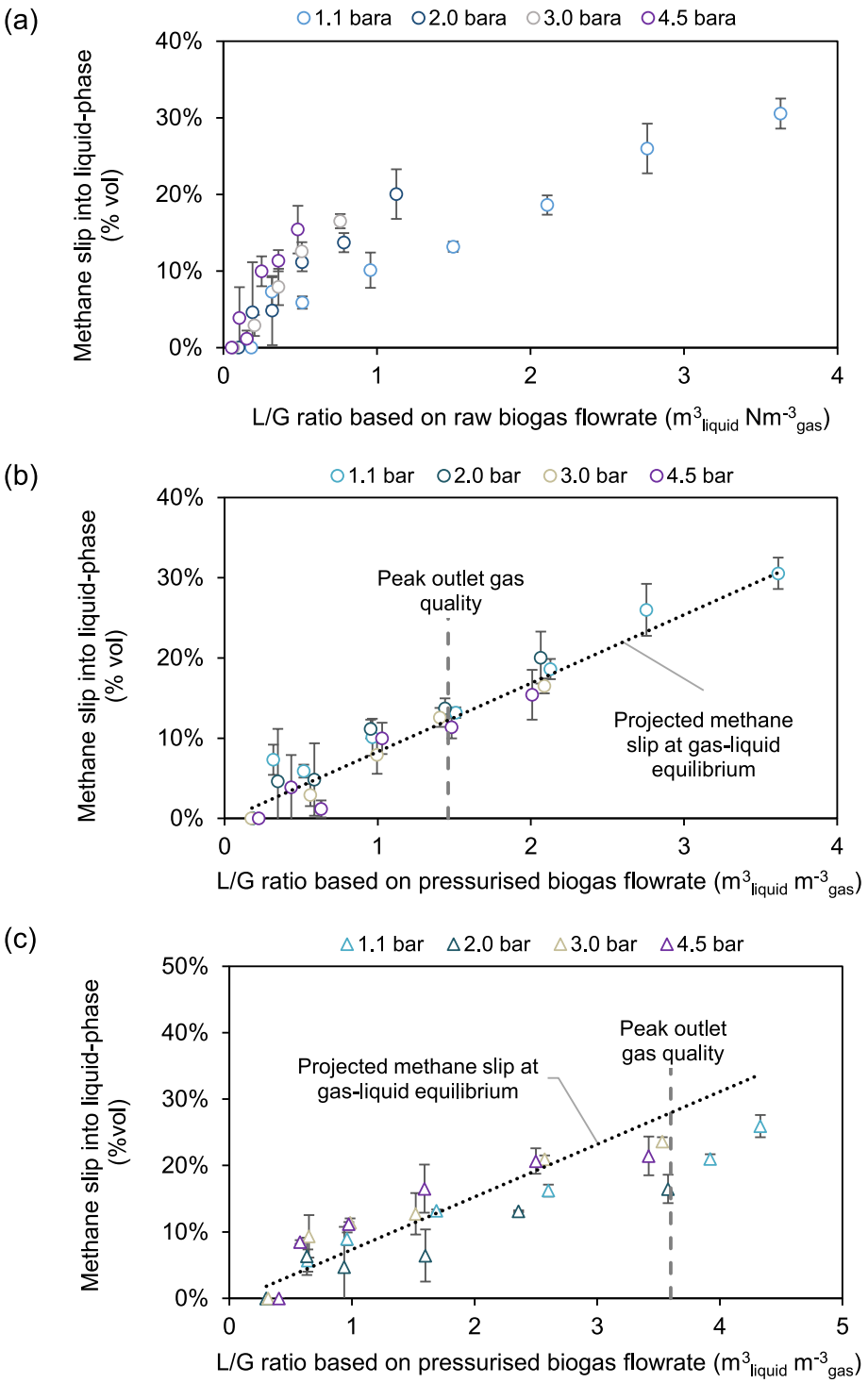

Fig. 12. Methane slip into liquid-phase within: (a) the microporous membrane (m^3_{liquid} Nm^{-3}_{gas}); (b) the microporous membrane normalised to pressure (m^3_{liquid} m^{-3}_{gas}); (c) the nonporous membrane normalised to pressure (m^3_{liquid} m^{-3}_{gas}). Conditions: gas feed = 0.5/0.5 CO_2/CH_4; v_G = 0.02 m s^{-1}; solvent temperature = 5–10 °C; gas temperature in = 21 °C. Dotted line represents projected slip. Dashed line indicates the L/G ratio at peak outlet gas quality for a specific condition (Fig. 9).

Pressurisation can enhance CO_2 selectivity to improve gas product quality and levelised cost of production (capital and operational savings) while also minimising methane losses through 'slip' and enhancing methane recovery which is of practical significance to the viability of HFMC for biogas upgrading. Future work could include a detailed economic evaluation examining interactions between membrane material and operational conditions, including the energy related to chilling and pressurisation, to enable direct comparison for biogas upgrading in HFMC and absorption columns. The final biomethane product must inevitably undergo pressurisation before use (typically 7 bar for gas grid injection, and up to 180 bar for automotive). Upstream gas pressurisation therefore prepares the biomethane for final use, while reducing the capital and operating cost of biomethane production. While pressurisation is shown to reduce the cost of nonporous membranes through an increase in flux, microporous HFMC have been demonstrated as an effective solution for low temperature high pressure applications within this study, and as such poly(4-methyl-1-pentene) based membranes are unlikely to compete economically unless they can be manufactured with

an ultrathin dense layer that offers comparable mass transfer without compromising mechanical strength and plasticisation behaviour. Existing nonporous membranes may still prove competitive for high temperature, high pressure CO_2 applications due to the enhancement in permeability, and comparative increased risk of wetting in microporous membranes.

Author statement

B. Luqmani: Conceptualization; Data curation; Formal analysis; Investigation; Methodology; Roles/Writing - original draft.

A. Brookes: Conceptualization; Funding acquisition; Supervision; Writing - review & editing.

A. Moore: Conceptualization; Funding acquisition; Supervision; Writing - review & editing.

P. Vale: Conceptualization; Funding acquisition; Supervision; Writing - review & editing.

M. Pidou: Conceptualization; Funding acquisition; Supervision; Writing - review & editing.

E. McAdam: Conceptualization; Data curation; Formal analysis; Funding acquisition. Investigation; Methodology; Project administration; Supervision; Writing - review & editing.

Declaration of competing interest

The authors declare that they have no known competing financial interests or personal relationships that could have appeared to influence the work reported in this paper.

Data availability

Data underlying this paper can be accessed at: https://doi.org/10.17862/cranfield.rd.22634158.v1.

Acknowledgements

We are grateful for the financial and technical support offered by Anglian Water, Northumbrian Water and Severn Trent Water. We also acknowledge the funding and training resource provided to Benjamin Luqmani from the Engineering and Physical Sciences Research Council through the STREAM Industrial Doctorate Centre. Data underlying this paper can be accessed at: https://doi.org/10.17862/cranfield.rd.22634158.v1.

Appendix A. Supporting equations

A.1. Temperature and pressure correction for bubble flowmeter measurement

$$Q_{G,out} = Q_{G,bubble}\left(\frac{P_{g,out}}{P_{g,in}}\right)\left(\frac{T_{g,in}}{T_{g,out}}\right) \tag{A1}$$

where $Q_{G,bubble}$ is the gas flowrate measured using the bubble flowmeter [$m^3\ s^{-1}$]; $P_{g,out}$ is the gas pressure at the point of measurement [1 bar]; $T_{g,out}$ is the gas outlet temperature at the point of measurement [K] and $T_{g,in}$ is the gas inlet temperature [K].

A.2. Gas-phase CO_2 concentration

$$C_g = \frac{n}{V} = \frac{P_g}{z\,R\,T_g} \tag{A2}$$

where n/V is the amount of CO_2 per unit volume [mol m^{-3}]; P_g is the total gas pressure [bar]; z is the compressibility factor for CO_2 [-] and T_g is the gas temperature [K].

A.3. Kelvin equation describing capillary condensation

$$ln\left(\frac{P_{eq}}{P_{sat}}\right) = -\left(\frac{2\,\gamma\,v_l}{R\,T\,x_{crit}}\right)\cos\theta \tag{A3}$$

where γ is the liquid surface tension (N m^{-1}); v_L is this liquid molar volume (m^3 mol^{-1}); and x_{crit} is the average pore diameter (m).

A.4. Arrhenius relationship for polymer permeability

$$P_d = P_{d,0}e^{\frac{-E_a}{RT}} \tag{A4}$$

where P_d is polymer permeability (barrer) $P_{d,0}$ is a constant (−) and E_a is the polymer activation energy (J mol^{-1}).

A.5. Calculating flux enhancement factor (E)

$$E = \frac{J_{CO2}}{J^{\circ}_{CO2}} \tag{A5}$$

where E is the flux enhancement factor and J°_{CO2} is the CO_2 flux at 1.1 bar.

A.6. Projected methane slip based upon gas-liquid equilibrium at HFMC outlet

$$CH_4\ slip = \frac{Q_L\,C^*_{CH4,L,out}}{Q_{G,in}C_{CH4,g,in}} \tag{A6a}$$

$$C^*_{CH4,L} = P_{CH4,out}\,\rho_L\,k^o_H\,e^{\left[c\left(\frac{1}{T_L}-\frac{1}{298.15}\right)\right]} \tag{A6b}$$

where $C^*_{CH4,L}$ is the equilibrium concentration of methane in the liquid-phase [mol m^{-3}]; ρ_L is density of pure water at the liquid temperature [kg m^{-3}]; $P_{CH4,out}$ is the partial pressure of methane in the gas outlet [bar]; k^o_H and c are the Henry's Law constant for methane in pure water at 298 K [0.0013 mol kg^{-1} bar^{-1}] and its temperature dependence constant [K] respectively (Sander, 2015); T_L is the liquid-phase temperature [K].

Appendix B. Evaluation of Graetz-Leveque solution accuracy

Liquid phase resistances from the Graetz-Leveque solution (Equation (5)) were projected over a range of liquid velocities at 5, 10, 20 and 35 °C (Figure B1). The error between the projected values and the experimental values was calculated and compared (Figure B2). A convergence between projected and experimental values to within ± 5000 s m^{-1} was observed above Gz = 15, providing an acceptable degree of accuracy. Application of the Graetz-Leveque solution under these conditions supported the deduction of gas-phase mass transfer resistances during binary gas experiments.

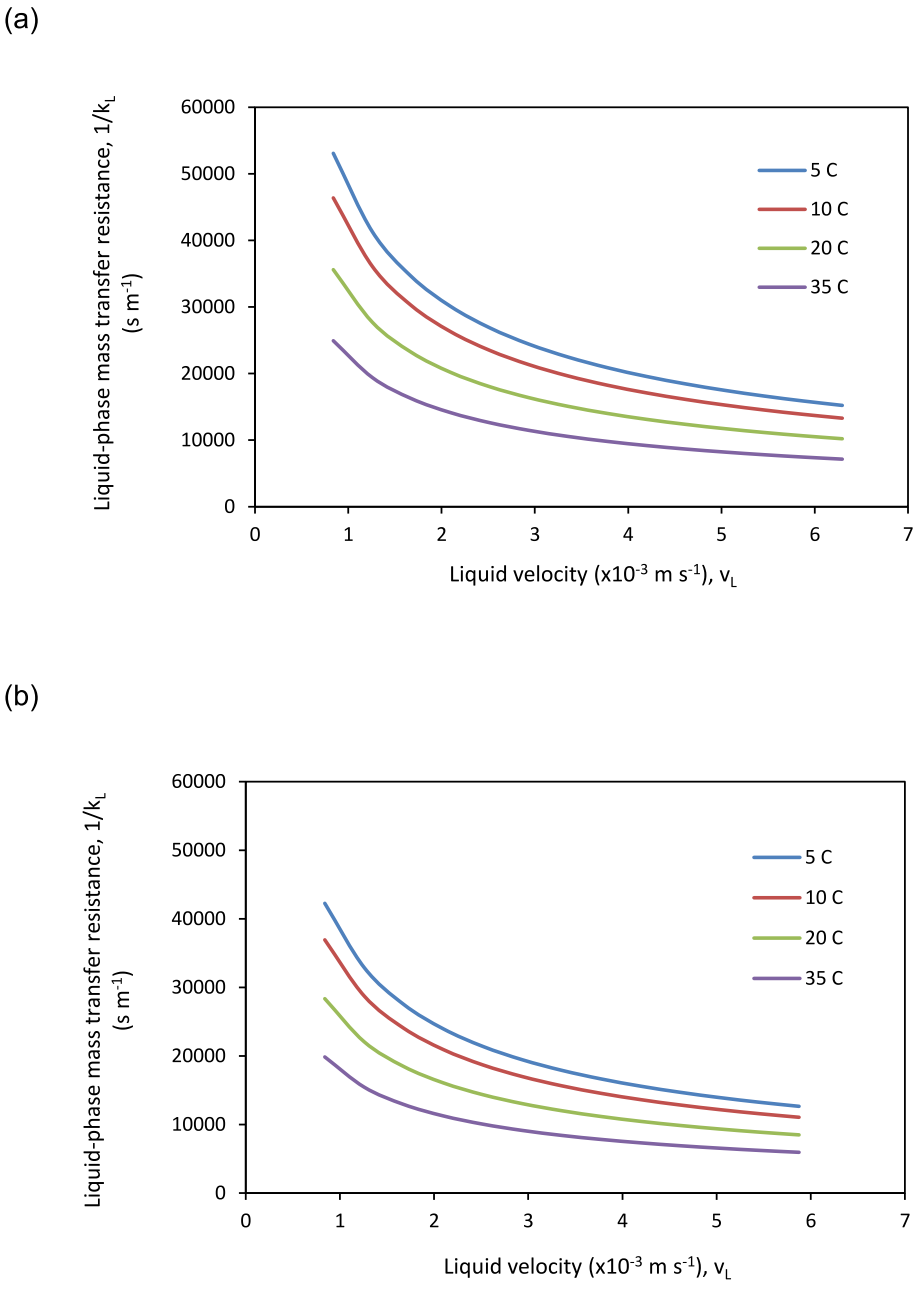

Fig. B1. Projected impact of temperature on liquid-phase mass transfer resistance for CO_2 transport from the liquid-membrane interface to the liquid bulk for the (a) microporous, and (b) nonporous membranes (Equation (5)).

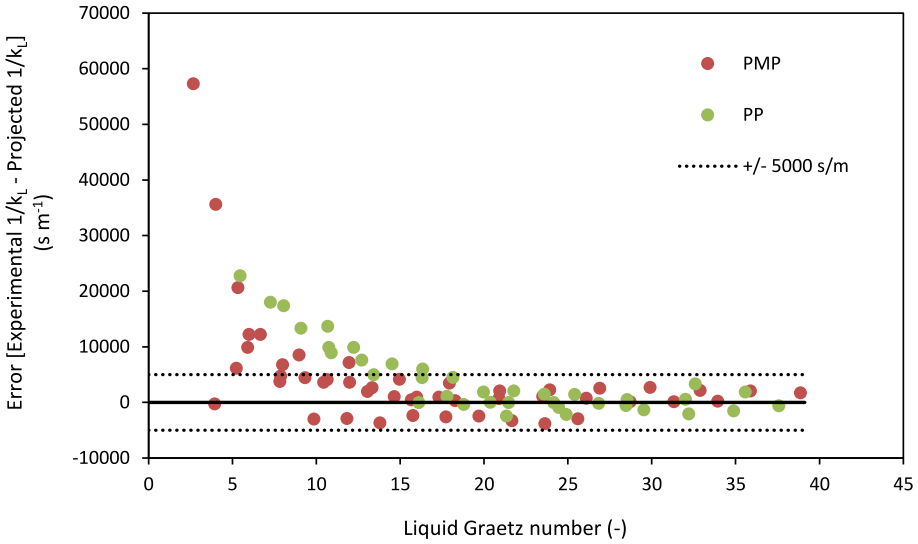

Fig. B2. Evaluation of Graetz-Leveque solution accuracy in the microporous (PP) and nonporous (PMP) membranes. Conditions: Pure CO_2 gas feed, $v_G = 0.07–0.08$ m s^{-1}, $P_g = 1.1$ bar, gas temperature in = 21 °C. Dotted lines at 5000 and -5000 s m^{-1} to represent typical error.

Appendix C. Impact of thinner dense-skins for non-porous module

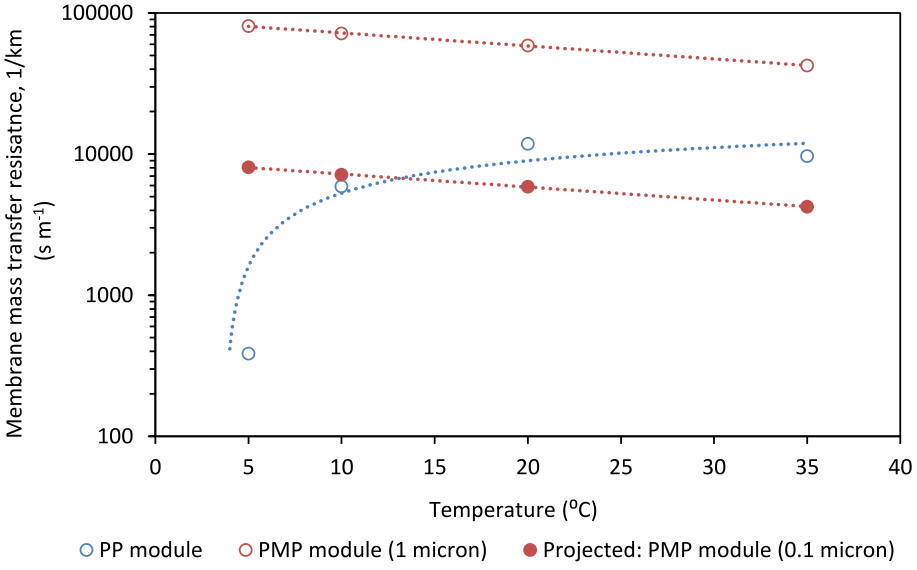

Fig. C1. Impact of reducing dense-skin thickness on membrane mass transfer resistance for the nonporous (PMP) module. Resistance at 0.1 μm dense-skin thickness projected based upon experimental permeability data (Equation (7)). Dotted lines added to guide the eye.

References

[1] F. Bauer, C. Hulteberg, T. Persson, D. Tamm, Biogas Upgrading – Review of Commercial Technologies, 2013. SGC, http://vav.griffel.net/filer/C_SGC2013-270.pdf. (Accessed 31 March 2023).

[2] N. Scarlat, J.F. Dallemand, F. Fahl, Biogas: developments and perspectives in Europe, Renew. Energy 129 (2018) 457–472.

[3] S. Alberici, M. Moultak, J. Peters, The Future Role of Biomethane, 2021. https://www.europeanbiogas.eu/wp-content/uploads/2022/01/The_future_role_of_biomethane-December_2021.pdf. (Accessed 31 March 2023).

[4] P.M. Connor, L. Xie, R. Lowes, J. Britton, T. Richardson, The development of renewable heating policy in the United Kingdom, Renew. Energy 75 (2015) 733–744.

[5] I. Angelidaki, L. Treu, P. Tsapekos, G. Luo, S. Campanaro, H. Wenzel, P.G. Kougias, Biogas upgrading and utilization: current status and perspectives, Biotechnol. Adv. 36 (2018) 452–466.

[6] IEA Bioenergy, Task 37: Energy from Biogas Upgrading Plant List 2019, International Energy Agency (2019). https://task37.ieabioenergy.com/plant-lists/. (Accessed 1 April 2023).

[7] K.A. Hoff, H.F. Svendsen, CO2 absorption with membrane contactors vs. packed absorbers- Challenges and opportunities in post combustion capture and natural gas sweetening, Energy Proc. 37 (2013) 952–960.

[8] B. Belaissaoui, J. Claveria-Baro, A. Lorenzo-Hernando, D. Albarracin Zaidiza, E. Chabanon, C. Castel, S. Rode, D. Roizard, E. Favre, Potentialities of a dense skin hollow fiber membrane contactor for biogas purification by pressurized water absorption, J. Membr. Sci. 513 (2016) 236–249.

[9] M. Mavroudi, S.P. Kaldis, G.P. Sakellaropoulos, A study of mass transfer resistance in membrane gas – liquid contacting processes, J. Membr. Sci. 272 (2006) 103–115.

[10] V.Y. Dindore, D.W.F. Brilman, P.H.M. Feron, G.F. Versteeg, CO2 absorption at elevated pressures using a hollow fiber membrane contactor, J. Membr. Sci. 235 (2004) 99–109.

[11] S. Khaisri, D. DeMontigny, P. Tontiwachwuthikul, R. Jiraratananon, Comparing membrane resistance and absorption performance of three different membranes in a gas absorption membrane contactor, Sep. Purif. Technol. 65 (2009) 290–297.

[12] R. Wang, H.Y. Zhang, P.H.M. Feron, D.T. Liang, Influence of membrane wetting on CO2 capture in microporous hollow fiber membrane contactors, Sep. Purif. Technol. 46 (2005) 33–40.

[13] C.A. Scholes, S.E. Kentish, G.W. Stevens, D. DeMontigny, Comparison of thin film composite and microporous membrane contactors for CO2 absorption into monoethanolamine, Int. J. Greenh. Gas Control 42 (2015) 66–74.
[14] Z.P. Chan, L. Li, G. Kang, N.A. Manan, Y. Cao, T. Wang, Discussion on water condensation in membrane pores during CO2 absorption at high temperature, Membranes 10 (2020) 407.
[15] K. Villeneuve, A.A. Torres Hernandez, D. Albarracin Zaidiza, D. Roizard, S. Rode, Effects of water condensation on hollow fiber membrane contactor performance for CO2 capture by absorption into a chemical solvent, J. Membr. Sci. 556 (2018) 365–373.
[16] S. Houlker, T. Rutherford, D. Herron, A. Brookes, A. Moore, P. Vale, M. Pidou, E. McAdam, Demonstrating commercial hollow fibre membrane contactor performance at industrial scale for biogas upgrading at a sewage treatment works, Water (Switzerland) 13 (2021) 172.
[17] L. Cesari, C. Castel, E. Favre, Membrane contactors for intensified gas-liquid absorption processes with physical solvents: a critical parametric study, J. Membr. Sci. 635 (2021), 119377.
[18] Z. Dai, L. Deng, Membrane absorption using ionic liquid for pre-combustion CO2 capture at elevated pressure and temperature, Int. J. Greenh. Gas Control 54 (2016) 59–69.
[19] A. Mansourizadeh, Experimental study of CO2 absorption/stripping via PVDF hollow fiber membrane contactor, Chem. Eng. Res. Des. 90 (2012) 555–562.
[20] J.G. Lu, Y.F. Zheng, M.D. Cheng, Wetting mechanism in mass transfer process of hydrophobic membrane gas absorption, J. Membr. Sci. 308 (2008) 180–190.
[21] S. Bavarella, B. Luqmani, N. Thomas, A. Brookes, A. Moore, P. Vale, M. Pidou, E. J. McAdam, CO2 absorption into aqueous ammonia using membrane contactors: role of solvent chemistry and pore size on solids formation for low energy solvent regeneration, Sep. Purif. Technol. 290 (2022), 120786.
[22] R. Kapoor, P.M.V. Subbarao, V.K. Vijay, Integration of flash vessel in water scrubbing biogas upgrading system for maximum methane recovery, Bioresource Technol. Reports 7 (2019), 100251.
[23] Q. Sun, H. Li, J. Yan, L. Liu, Z. Yu, X. Yu, Selection of appropriate biogas upgrading technology-a review of biogas cleaning, upgrading and utilisation, Renew. Sustain. Energy Rev. 51 (2015) 521–532.
[24] J. Läntelä, S. Rasi, J. Lehtinen, J. Rintala, Landfill gas upgrading with pilot-scale water scrubber: performance assessment with absorption water recycling, Appl. Energy 92 (2012) 307–314.
[25] S. Rasi, J. Läntelä, A. Veijanen, J. Rintala, Landfill gas upgrading with countercurrent water wash, Waste Manag. 28 (2008) 1528–1534.
[26] Northern Gas Networks, Biomethane: a Producer's Handbook, 2020. https://biomethane.northerngasnetworks.co.uk/wp-content/uploads/2020/07/NGN_BiomethaneHandbook_0420_St04A.pdf. (Accessed 31 March 2023).
[27] L. Yang, X. Ge, C. Wan, F. Yu, Y. Li, Progress and perspectives in converting biogas to transportation fuels, Renew. Sustain. Energy Rev. 40 (2014) 1133–1152.
[28] S. Houlker, Scale up of Hollow Fibre Membrane Contactors for Biogas Upgrading. EngD Thesis, 2019. Cranfield University.
[29] E. Chabanon, B. Belaissaoui, E. Favre, Gas-liquid separation processes based on physical solvents: opportunities for membranes, J. Membr. Sci. 459 (2014) 52–61.
[30] P.T. Nguyen, E. Lasseuguette, Y. Medina-Gonzalez, J.C. Remigy, D. Roizard, E. Favre, A dense membrane contactor for intensified CO2 gas/liquid absorption in post-combustion capture, J. Membr. Sci. 377 (2011) 261–272.
[31] J.M. Mohr, D.R. Paul, Effect of casting solvent on the permeability of poly (4-methyl-1-pentene), Polymer 32 (1991) 1236–1243.
[32] M.H. Nematollahi, A.H.S. Dehaghani, R. Abedini, CO2/CH4 separation with poly (4-methyl-1-pentyne) (TPX) based mixed matrix membrane filled with Al2O3 nanoparticles, Kor. J. Chem. Eng. 33 (2016) 657–665.
[33] G.Q. Chen, C.A. Scholes, C.M. Doherty, A.J. Hill, G.G. Qiao, S.E. Kentish, Modeling of the sorption and transport properties of water vapor in polyimide membranes, J. Membr. Sci. 409 (410) (2012) 96–104.
[34] C.A. Scholes, S. Kanehashi, G.W. Stevens, S.E. Kentish, Water permeability and competitive permeation with CO2 and CH4 in perfluorinated polymeric membranes, Sep. Purif. Technol. 147 (2015) 203–209.
[35] S. Markova, M. Shalygin, M. Pelzer, T. Gries, V. Teplyakov, Application prospects of dense gas separation hollow fibers based on poly (4-methyl-1-pentene), Chem. Pap. 74 (2020) 1917–1921.
[36] G.C. Kapantaidakis, G.H. Koops, M. Wessling, S.P. Kaldis, G.P. Sakellaropoulos, CO2 plasticization of polyethersulfone/polyimide gas-separation membranes, AIChE J. 49 (2003) 1702–1711.
[37] 3M, Liqui-Cel EXF Series Membrane Contactors - Cleaning and Storage Guidelines, 2023. https://multimedia.3m.com/mws/media/2282742O/pdf-of-the-cleaning-and-storage-guidelines-for-the-3m-liqui-cel-exf-membrane-contactors.pdf. (Accessed 24 April 2023).
[38] A. Gabelman, S. Hwang, Hollow fiber membrane contactors, J. Membr. Sci. 159 (1999) 61–106.
[39] Z. Cui, D. Demontigny, Part 7: a review of CO2 capture using hollow fiber membrane contactors, Carbon Manag. 4 (2013) 69–89.
[40] S. Shen, S.E. Kentish, G.W. Stevens, Shell-side mass-transfer performance in hollow-fiber membrane contactors, Solvent Extr. Ion Exch. 28 (2010) 817–844.
[41] A. Baudot, J. Floury, H.E. Smorenburg, Liquid-liquid extraction of aroma compounds with hollow fiber contactor, AIChE J. 47 (2001) 1780–1793.
[42] S. Houlker, C.J. Davey, A. Allemand, A. Brookes, A. Moore, P. Vale, M. Pidou, E. J. McAdam, Reconciliation of gas to liquid mass transfer in parallel and transverse flow (cross-flow) hollow fiber membrane contactors (HFMC) for CO2 absorption, Separ. Sci. Technol. 56 (2021) 129–140.
[43] E. Chabanon, D. Roizard, E. Favre, Modeling strategies of membrane contactors for post-combustion carbon capture : a critical comparative study, Chem. Eng. Sci. 87 (2013) 393–407.
[44] S. Heile, C.A.L. Chernicharo, E.M.F. Brandt, E.J. McAdam, Dissolved gas separation for engineered anaerobic wastewater systems, Sep. Purif. Technol. 189 (2017) 405–418.
[45] S. Atchariyawut, C. Feng, R. Wang, R. Jiraratananon, D.T. Liang, Effect of membrane structure on mass-transfer in the membrane gas–liquid contacting process using microporous PVDF hollow fibers, J. Membr. Sci. 285 (2006) 272–281.
[46] H. Mahmud, A. Kumar, R.M. Narbaitz, T. Matsuura, A study of mass transfer in the membrane air-stripping process using microporous polypropylene hollow fibers, J. Membr. Sci. 179 (2000) 29–41.
[47] Z. Mohamad, H. Mohd, A.L. Ahmad, S. Rode, B. Belaissaoui, D. Roizard, S.C. Low, U.D.L. Cnrs, G. Bp, N. Cedex, Prospect of oxyplus hollow fibre membrane with dense polymethylpentene (PMP) skin as support-gutter layer of thin film composite (TFC) for biogas upgrading, J. Phys. Sci. 30 (2019) 179–189.
[48] C. Makhloufi, D. Roizard, E. Favre, Reverse selective NH3/CO2 permeation in fluorinated polymers using membrane gas separation, J. Membr. Sci. 441 (2013) 63–72.
[49] H. Yasuda, K. Rosengren, Isobaric measurement of gas permeability of polymers, J. Appl. Polym. Sci. 14 (1970) 2839–2877.
[50] X. Feng, R.Y.M. Huang, Estimation of activation energy for permeation in pervaporation processes, J. Membr. Sci. 118 (1996) 127–131.
[51] B. Tansel, S.C. Surita, Managing siloxanes in biogas-to-energy facilities: economic comparison of pre- vs post-combustion practices, Waste Manag. 96 (2019) 121–127.
[52] M. Kattula, K. Ponnuru, L. Zhu, W. Jia, H. Lin, E.P. Furlani, Designing ultrathin film composite membranes: the impact of a gutter layer, Nature Scientific Reports 5 (2015), 15016.
[53] Intergovernmental Panel on Climate Change (IPCC), Changes in Atmospheric Constituents and in Radiative Forcing, 2007. http://www.ipcc.ch/publications_and_data/ar4/wg1/en/ch2s2-10-2.html. (Accessed 31 March 2023).
[54] A. McLeod, B. Jefferson, E.J. McAdam, Quantifying the loss of methane through secondary gas mass transport (or 'slip') from a micro-porous membrane contactor applied to biogas upgrading, Water Res. 47 (2013) 3688–3695.
[55] R.W. Bucklin, R.L. Schendel, Comparison of physical solvents used for gas processing, in: S.A. Newman (Ed.), Acid and Sour Gas Treating Processes, Gulf Publishing Company, Houston, TX, USA, 1985, pp. 42–48.
[56] T. Kvist, N. Aryal, Methane loss from commercially operating biogas upgrading plants, Waste Manag. 87 (2019) 295–300.
[57] T. Patterson, S. Esteves, R. Dinsdale, A. Guwy, An evaluation of the policy and techno-economic factors affecting the potential for biogas upgrading for transport fuel use in the UK, Energy Pol. 39 (2011) 1806–1816.